Journal of Materials Chemistry

Dynamic Article Links

Cite this: *J. Mater. Chem.*, 2012, **22**, 2254

www.rsc.org/materials

PAPER

Quasi-seeded growth, phase transformation, and size tuning of multifunctional hexagonal $NaLnF_4$ (Ln = Y, Gd, Yb) nanocrystals *via in situ* cation-exchange reaction†

L. W. Yang,*[ab] Y. Li,[a] Y. C. Li,[a] J. J. Li,[a] J. H. Hao,*[b] J. X. Zhong[a] and P. K. Chu*[c]

Received 7th September 2011, Accepted 3rd November 2011
DOI: 10.1039/c1jm14425a

In situ cation exchange between alkali ions in ternary alkali lanthanide (Ln^{3+}) fluoride on the nanoscale is reported. Experimental results reveal that the differences in the solubility constants and thermodynamic stability of the reactants and products affect the irreversible cation exchange between potassium and sodium, resulting in the phase transformation of cubic $KLnF_4$ to hexagonal $NaLnF_4$. The unusual cation-exchange reaction can be used as an efficient tool to produce seed nuclei and control the nucleation and final size of hexagonal $NaLnF_4$ nanocrystals (NCs). During the *in situ* cation exchange between potassium and sodium and corresponding cubic to hexagonal phase transformation, the stable hexagonal $NaLnF_4$ particles serving as the seed nuclei play a key role in the final size of the NCs. The *in situ* cation exchange approach provides not only valuable insights into the growth dynamics of Ln^{3+} doping-induced size tuning and phase transformation in $NaYF_4$ and alkaline-earth fluoride NCs, but also a method to prepare high-quality multifunctional $NaLnF_4$ NCs with tunable paramagnetism and multi-color upconversion emission.

1. Introduction

Interests in lanthanide (Ln^{3+}) doped fluoride nanocrystals (NCs) have been increasing due to their unique upconversion (UC) properties and potential applications for solid-state lasers,[1] multi-color displays,[2,3] solar cells,[4] and especially bio-labels for biological assays, medical imaging, and photodynamic therapy.[5–7] At present, efforts have been devoted to the control of the size, shape, and composition of NCs to realize multicolor UC emission and multifunctionality.[3,8–23] The ability to do so is necessary in order to expedite applications for optical–magnetic dual-modal biomedical imaging. It has been demonstrated that paramagnetism and multi-color UC emission spanning infrared to deep ultraviolet including white light can be obtained from fluoride NCs by precisely controlling the Ln^{3+} doping type and concentration together with the introduction of paramagnetic Gd^{3+} ions.[13–15,18,22,24–28] Moreover, several groups have reported applications to biology including both *in vitro* and *in vivo* imaging.[22,24–26] However, there is still a lack of clear understanding of the size dependent physical properties, especially the paramagnetic properties of these multifunctional NCs. Furthermore, it is important to prepare multifunctional NCs with uniform composition and size between 100 and 10 nm.

Impurity doping has recently been found to influence the growth of multifunctional NCs.[3,21,29,30] For instance, Liu and co-workers demonstrated that the size, phase, and UC emission color of $NaYF_4$ NCs could be tuned by introducing trivalent Ln^{3+} dopant ions such as Gd^{3+}, Sm^{3+} and Nd^{3+}.[3] Similar phenomena concerning size tuning and phase transformation were observed from MF_2 (M = Ba, Sr, Ca) and LnF_3 NCs by heterovalent M^{2+} and Ln^{3+} doping, respectively.[21,30] However, knowledge on the formation of doped NCs is still limited. According to first-principle calculation, Liu *et al.*[3] proposed that the influence of lanthanide doping on the crystal phase and size arose from a strong dependence on the size and dipole polarizability of the substitutional dopant. Chen *et al.* considered that size tuning of the NCs arose from the transient electric dipole induced by heterovalent doping, which could modify the diffusion of F^- ions from the solution to grain surface thereby retarding the growth of Ln^{3+}-doped MF_2 NCs.[21,30] Despite these efforts, the dynamic process and interactions between dopant ions and host lattices during the growth of doped NCs are not fully understood.

Cation exchange was first reported in the reaction of Ag with CdSe nanoparticles at room temperature by Alivisatos *et al.*[31] Following this discovery, many different types of functional

[a]*Laboratory for Quantum Engineering and Micro-Nano Energy Technology and Faculty of Materials and Optoelectronic Physics, Xiangtan University, Hunan, 411105, China. E-mail: ylwxtu@xtu.edu.cn*
[b]*Department of Applied Physics, The Hong Kong Polytechnic University, Hong Kong, China. E-mail: apjhhao@polyu.edu.hk*
[c]*Department of Physics and Materials Science, City University of Hong Kong, Tat Chee Avenue, Kowloon, Hong Kong, China. E-mail: paul.chu@cityu.edu.hk*

† Electronic supplementary information (ESI) available. See DOI: 10.1039/c1jm14425a

nanomaterials, including hollow PbSe nanospheres, superlattices of CdS–Ag_2S on nanorods and core–shell nanoparticles of Se–Ag_2Se, Se–CdSe, Se–PbSe, and PbSe–CdSe, have been prepared in solution *via* cation exchange reactions.[32–36] Recently, Veggel *et al.* reported that cation exchange also occurred in LnF_3 NCs in aqueous dispersions even at room temperature.[37] However, to our knowledge, cation exchange in ternary $ALnF_4$ (A = Li, Na or K) on the nanoscale, for example, ternary $NaLnF_4$ NCs (known to be the most efficient hosts for UC emission) *via in situ* cation exchange, has not been reported.

In this work, we investigate *in situ* cation exchange between alkali ions on the nanoscale in ternary $ALnF_4$ and illustrate an approach to control the growth rate of hexagonal $NaLnF_4$ NCs *via* the introduction of intermediate reactants that undergo an ion-exchange reaction and form the final $NaLnF_4$ product in a liquid–solid-solution (LSS) reaction system. We demonstrate that mediated nucleation followed by cation exchange can determine the overall nucleation rate and final size of the hexagonal $NaLnF_4$ NCs. Our results provide not only valuable insights into the growth dynamics of Ln^{3+} doping-induced size tuning and phase transformation in $NaYF_4$ and MF_2 NCs, but also a method to prepare high-quality multifunctional $NaLnF_4$ NCs with tunable paramagnetism and multi-color UC emission.

2. Experimental details

2.1 Materials

The synthesis was carried out using commercially available reagents. The $Ln(NO_3)_3 \cdot 6H_2O$ was 99.99% pure and supplied by Sinopharm Chemical Reagent Company. All the other chemicals were analytical grade and used as received without further purification.

2.2 Synthesis of $NaLnF_4$ and $KLnF_4$ NCs

In a typical synthesis, 2 ml of an aqueous solution containing 8.75 mmol NaOH or KOH, 10 ml of alcohol, and 20 ml of oleic acid (OA) were added to a beaker sequentially under vigorous stirring to form a transparent homogeneous solution at room temperature. Afterwards, 2.24 ml of 0.5 M of $Ln(NO_3)_3$ (1.12 mmol) with predesigned Yb^{3+} and Er^{3+} doping concentrations were poured into the translucent solution under vigorous stirring. The mixture was aged for 10 min at room temperature and then 5 ml of 1.2 M NH_4F was added under vigorous stirring until a translucent solution was obtained. After agitating for another 30 min, the colloidal solution was transferred to a 50 ml stainless Teflon-lined autoclave. The reactions were conducted in an oven at 180–210 °C for 24 h. After the reaction, the products deposited on the bottom of the Teflon vessel were collected, washed with ethanol and deionized water several times to remove other remnants, and then dried at 70 °C for 24 h.

2.3 Cation exchange of K^+ by Na^+ in Yb^{3+}/Er^{3+} codoped $KLnF_4$ NCs

The aforementioned experimental procedures were first conducted for a reaction time of about 20 h. The mixture was cooled to 100 °C. Subsequently, another semitransparent solution containing the predesigned NaOH and OA contents was quickly added to the solution, rapidly heated to 180 °C, and maintained at this temperature for 2–20 h. After the reaction, the products deposited on the bottom of the Teflon vessel were collected, washed with ethanol and deionized water several times, and dried at 70 °C for 24 h.

2.4 *In situ* cation exchange of K^+ by Na^+ in $KLnF_4$, $KYb_{0.55}Gd_{0.45}F_4$ and $KY_{0.55}Gd_{0.45}F_4$ NCs

In the typical process, 2 ml of an aqueous solution containing 8.75 mmol KOH, 10 ml of alcohol, and 20 ml of OA were added to a beaker sequentially under vigorous stirring to form a transparent homogeneous solution at room temperature. Then, 2.24 ml of 0.5 M of $Ln(NO_3)_3$ (1.12 mmol) with the predesigned Gd^{3+},$Y^{3+}$and Yb^{3+} contents were poured into the translucent solution under vigorous stirring. After aging for 10 min at room temperature, 4 ml of an aqueous solution containing 6 mmol NH_4F was added under vigorous stirring until a translucent solution was obtained. The mixture was aged for another 30 min to form the amorphous precursor at room temperature. Before transferring to a Teflon-lined autoclave with an internal volume of 50 mL, the solution was mixed with another semitransparent solution containing predesigned NaOH and OA contents. The reaction was conducted in an oven at 180–210 °C for 0–40 h. After the reaction, the products deposited on the bottom of the Teflon vessel were collected, washed with ethanol and deionized water several times, and dried at 70 °C for 24 h.

2.5 Synthesis of Ln^{3+} doped $NaY_{0.55}Gd_{0.45}F_4$ and $NaYb_{0.55}Gd_{0.45}F_4$ NCs

The experimental procedures described in Section 2.4 were used to prepared the Ln^{3+} doped $NaY_{0.55}Gd_{0.45}F_4$ and $NaYb_{0.55}Gd_{0.45}F_4$ NCs by simply adjusting the constituents of $Ln(NO_3)_3$ solution.

2.6 Characterization

The crystal structures of the synthesized samples were determined by powder X-ray diffraction (D/Max 8550) using a copper K_α radiation source ($\lambda = 0.154$ nm) at 40 kV and 40 mA. The morphology and microstructure were characterized by transmission electron microscopy (TEM, JEOL 2100) equipped with selected area electron diffraction (SAED) and an Oxford energy dispersive X-ray spectroscopy (EDS) system at an acceleration voltage of 200 KV. The TEM specimens were prepared by directly drying a drop of a diluted cyclohexane dispersion solution of the as-prepared products on the surface of a carbon-coated copper grid. The UC spectra were recorded on a spectrophotometer (R-500) under the excitation of a 980 nm laser diode with an output power of about 1.0 W after the powder samples were compressed into smooth slices. The fluorescence spot of the parallel laser beam on the sample had a diameter of about 0.4 cm and the measurements were performed at room temperature. The UC photographic images were taken by a digital camera (Canon PowerShot A720, Japan) without a filter. The magnetization as a function of applied magnetic field ranging from −15 to 15 kOe was measured using a Lakeshore vibrating sample magnetometer (VSM) at room temperature.

3. Results and discussion

3.1 Crystal phase and size evolution during *in situ* cation exchange

In our preliminary experiments, we observed an obvious cation-exchange reaction during the treatment of preformed oleate-capped nearly spherical-shaped cubic $KYb_{0.1}Gd_{0.9}F_4$ NCs (see Fig. S1) with NaOH, NaOA, or NaCl in an aqueous ethanol solution. According to the EDS results of the oleate-capped cubic $KYb_{0.1}Gd_{0.9}F_4$ NCs treated with NaOA for different periods of time at 180 °C (see Fig. S2†), as the reaction proceeds, the potassium content decreases gradually and finally disappears, suggesting the occurrence of cation exchange between potassium and sodium. The powder XRD patterns (see Fig. S3†) of the oleate-capped cubic $KYb_{0.1}Gd_{0.9}F_4$ NCs treated with NaOA for different periods of time at 180 °C indicate that in the initial stage (reaction time of 2 h), the XRD peak position of the cubic phase shifts to a high angle. The calculated cell constants become smaller, implying that the cubic $KGdF_4$ NCs have partially transformed into cubic $NaGdF_4$ *via* cation exchange since the ionic radius of Na^+ is smaller than that of K^+. As the reaction proceeds further, hexagonal $NaGdF_4$ emerges. When the reaction time is longer than 20 h, all the diffraction peaks belonging to the cubic phase vanish almost completely, and pure hexagonal $NaGdF_4$ is formed. The results reveal that hexagonal $NaGdF_4$ is more thermodynamically stable than cubic $KGdF_4$ and cubic $KGdF_4$ NCs can be converted into a hexagonal phase *via* an intermediate cubic one due to cation exchange between K^+ and Na^+.

This phenomenon enables *in situ* ion exchange during the nucleation stage by introducing NaOA or NaCl with different contents directly into the precursor solution in the synthesis of cubic $KGdF_4$ NCs. This enables the formation of cubic NC and then the hexagonal NC transformation. Fig. 1a shows the XRD patterns of the $NaYb_{0.1}Gd_{0.9}F_4$ samples synthesized for different periods of time at 180 °C using precursors with a potassium : sodium molar ratio of 94 : 6. No crystal phase is found from the precursors and mixed hexagonal and cubic phases appear after 2 h. By increasing the reaction time to 40 h and beyond, all diffraction peaks belonging to the cubic phase disappear and the pure hexagonal phase (β-$NaGdF_4$) is formed. In addition, compared to the broad diffraction peaks of the cubic phase, the XRD pattern of the β-$NaGdF_4$ product becomes much sharper, implying a larger crystal size. When changing the molar ratio of potassium : sodium from 100 : 0 to 90 : 10 at a fixed reaction temperature of 180 °C and time of 20 h, the XRD shows similar phase transformation from the pure cubic phase to the mixed cubic and hexagonal one and finally the pure hexagonal one (see Fig. S4†). It should be pointed out that with increasing the amounts of sodium in the precursors, the duration for complete transformation from cubic to hexagonal phase is notably reduced. For the samples obtained from the precursors with a potassium : sodium molar ratio of 90 : 10, it takes only 5 h to realize the above phase transformation (see Fig. S5†). The results reveal that the cubic phase is a metastable phase, whereas the β-$NaGdF_4$ phase is thermodynamically stable during the reaction when the precursors include both potassium and sodium. This is completely different from the case that high-quality cubic $KGdF_4$ NCs are stable when the precursors contain potassium solely. The precursor to the cubic phase and then the hexagonal phase transformation are further characterized by TEM, EDS, and XPS. Fig. 1b shows a typical TEM image of the sample synthesized using precursors with a potassium : sodium molar ratio of 94 : 6 for 20 h. The as-prepared sample is composed of two distinct structures including small NCs with a diameter of about 10 nm and large rods with a diameter of about 130 nm, as verified by the two phases observed by XRD. The EDS results (Fig. 1c) reveal that the major chemical constituents of small NCs (Part A) are K, Na Yb, Gd, and F, whereas the major ones in the large rods are Na, Yb Gd, and F. The corresponding SAED

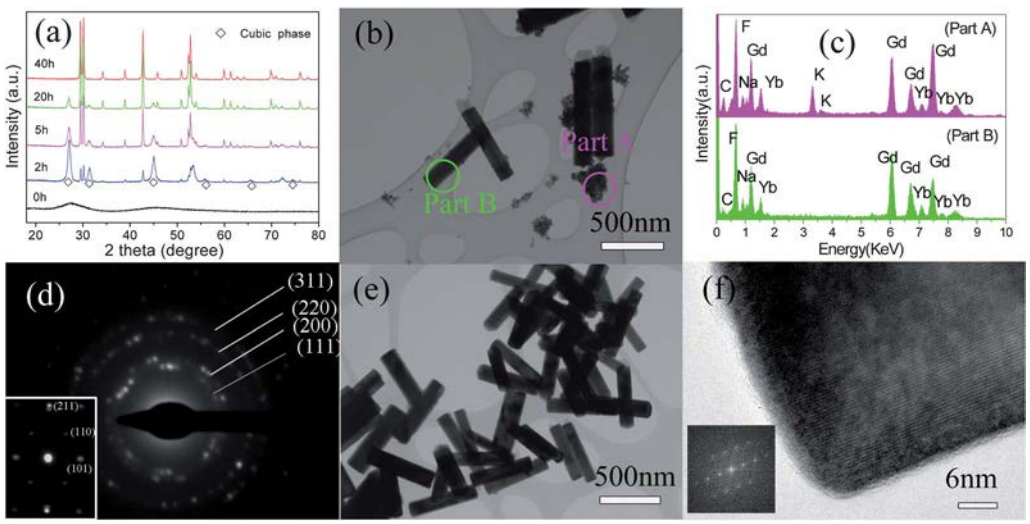

Fig. 1 (a) XRD patterns of the $NaYb_{0.1}Gd_{0.9}F_4$ sample synthesized for different times at 180 °C using precursors with a potassium : sodium ratio of 94 : 6. (b) and (e) Typical TEM images of the samples synthesized using precursors with a potassium : sodium ratio of 94 : 6 for 20 and 40 h, respectively. (c) EDS spectra of the areas marked Part A and Part B in (b). (d) SAED patterns of the areas marked Part A and Part B (see the inset) in (b), respectively. (f) A HR-TEM image of a single nanorod synthesized for 40 h. The inset is the corresponding FFT patterns.

patterns in Fig. 1d show that the small NCs are cubic $KGdF_4$ and $NaGdF_4$, but the large rods are hexagonal $NaGdF_4$. Fig. 1e shows a typical TEM image of the sample synthesized using precursors with a potassium : sodium molar ratio of 94 : 6 for 40 h. Only rods with an average diameter of about 135 nm are observed. The high-resolution TEM (HR-TEM) image (see Fig. 1f) discloses that the rods have a highly-crystalline hexagonal phase. The distance between the fringes (*d*-spacing) is ~5.22 Å, which corresponds to the distance of the (100) plane of standard hexagonal $NaGdF_4$. The detailed XPS analyses of the sample synthesized for 40 h shown in Fig. 2 indicates that there is no detectable K in the final rods that are just composed of Na, Yb, Gd, and F. This is different from $KYb_{0.1}Gd_{0.9}F_4$ NCs (see Fig. S6†). Hence, the phase transformation between cubic $KGdF_4$ and hexagonal $NaGdF_4$ occurs *via* an intermediate cubic $NaGdF_4$ one due to *in situ* cation exchange between potassium and sodium. It is similar to that observed for the oleate-capped cubic $KGdF_4$ NCs treated with NaOA.

Fig. 3(a) shows the XRD patterns of $NaYb_{0.1}Gd_{0.9}F_4$ samples synthesized for 20 h at 180 °C using precursors with potassium : sodium molar ratios of 90 : 10, 80 : 20, 60 : 40, 40 : 60, and 20 : 80. All the XRD peaks can be indexed to the hexagonal phase $NaGdF_4$ and no extra diffraction peaks of cubic $KGdF_4$ can be observed, implying a complete cubic to hexagonal transformation. More importantly, by increasing the Na^+ concentrations in the precursors, the diffraction peaks gradually broaden suggesting a reduced average crystallite size. Fig. 3(b)–(f) show the representative TEM images of the samples synthesized using precursors with potassium : sodium molar ratios of 90 : 10, 80 : 20, 60 : 40, 40 : 6 0, and 20 : 80, respectively. Nanorods are observed and with increasing Na^+ concentrations, nananorods with gradually decreasing diameters from 100 to 10 nm are formed, as consistent with the XRD results. The results indicate that the size of hexagonal $NaGdF_4$ with uniform composition can be tuned by simply adjusting the Na^+ concentrations. This is highly desirable and enables better understanding of the size-dependent physical properties of multifunctional $NaGdF_4$ NCs.

To demonstrate the universal nature of this phase transformation and the corresponding size tuning *via in situ* cation exchange, we extend the experimental study to the other systems. By using the same procedures, the samples using the precursors containing Na, K, Y, F or Na, K, Yb, F with different potassium : sodium molar ratios are prepared at 190 °C for a reaction time of 20 h and then characterized using XRD. Similar cubic-to-hexagonal phase transformations are observed when the reaction time is longer than 20 h, as shown by the XRD results (Figs S7 and S8†). However, under the same conditions, the potassium : sodium molar ratio is smaller than that of $NaGdF_4$, because β-$NaGdF_4$ is more energetically stable and easily obtained than hexagonal phase $NaYF_4$ and $NaYbF_4$.[38] We also synthesize $NaYbF_4$ samples for 20 h using precursors with potassium : sodium molar ratios of 90 : 10, 80 : 20, 70 : 30, and 60 : 40. When the temperature is 210 °C, no obvious size tuning phenomena are observed although only pure hexagonal $NaYbF_4$ is formed (see XRD results in Fig. S9†). However after doping with the light Ln^{3+} ion Gd^{3+} with a content of 45%, a similar size tuning phenomenon occurs (see XRD results and TEM images in Fig. S10†). The results indicate that Gd^{3+} doping plays a key role in the size tuning of $NaYbF_4$ during *in situ* cation exchange and the corresponding phase transformation.

3.2 Quasi-seeded growth mechanism for crystal phase and size evolution

In principle, cation exchange can take place in a solution due to the difference of the solubility product (K_{sp}) between $NaLnF_4$

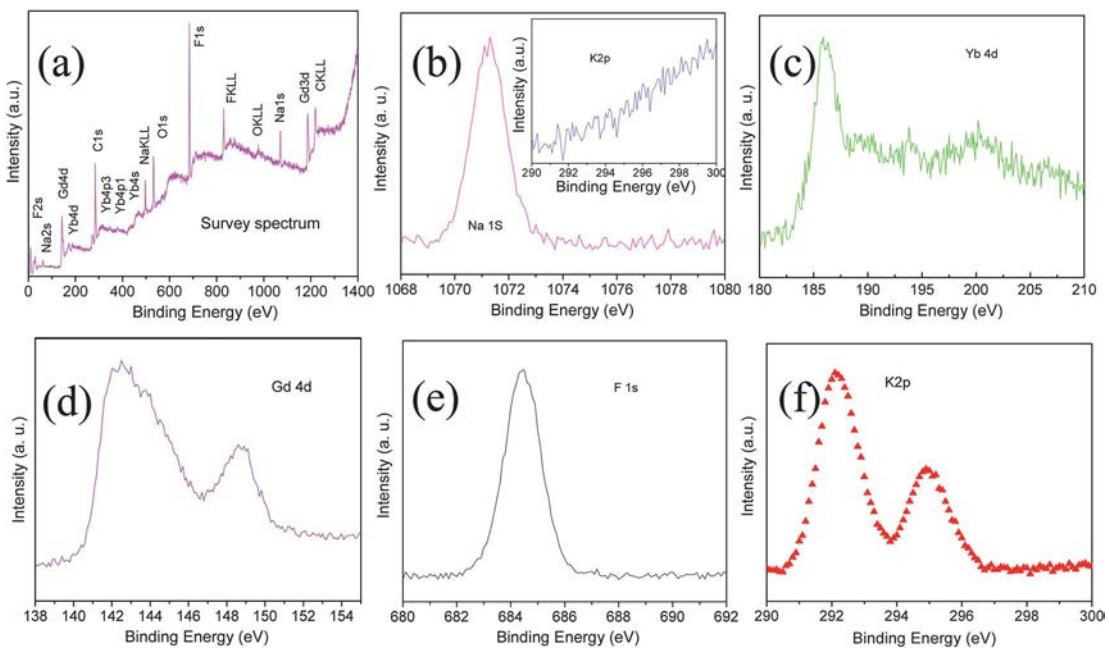

Fig. 2 (a) An XPS survey spectrum of the $NaYb_{0.1}Gd_{0.9}F_4$ sample synthesized at 180 °C for 40 h using precursors with a potassium : sodium ratio of 94 : 6. (b)–(e) Corresponding Na 1s, Yb 4d, Gd 4d, F1s XPS spectra. The inset in (b) is the XPS spectrum of the K 2p core level. (f) K 2p XPS spectra taken from the $KGdF_4$ NCs sample. The C 1s peak is used as the reference.

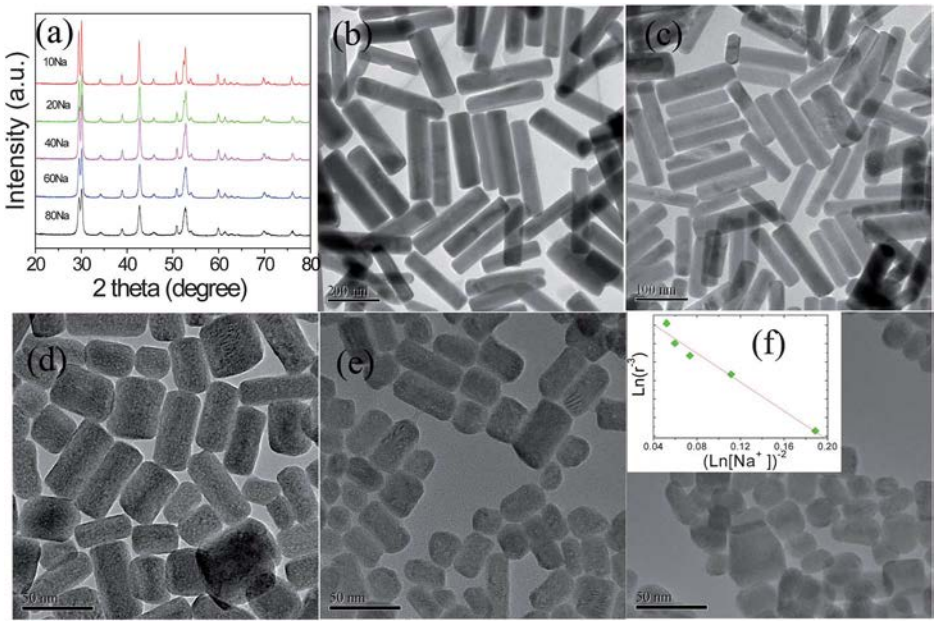

Fig. 3 (a) XRD patterns of the $NaYb_{0.1}Gd_{0.9}F_4$ samples synthesized for 20 h at 180 °C using precursors with potassium : sodium molar ratios of 90 : 10, 80 : 20, 60 : 40 and 40 : 60; 20 : 80, respectively. (b), (c), (d), (e) and (f) Typical TEM images of the samples using precursors with potassium : sodium molar ratios of 90 : 10, 80 : 20, 60 : 40 and 40 : 60, 20 : 80, respectively. The inset in (f) shows the experimental relationship between the Na^+ concentration and average size of the resulting $NaYb_{0.1}Gd_{0.9}F_4$ NCs, this is $\ln(r^{-3})$ *versus* $[\ln(Na^+)]^{-2}$.

and $KLnF_4$. Although the solubility products of ternary $ALnF_4$ are not readily found in the literature, qualitative K_{sp} values can be estimated by taking the value of alkali fluoride as a rough reference. Since the solubility of alkali fluoride is $K_{sp}(NaF) < K_{sp}(KF)$, one can infer that the solubility products of ternary $ALnF_4$ would have a lower value as the ionic radius of the alkali decreases, that is, $K_{sp}(NaLnF_4) < K_{sp}(KLnF_4)$. Furthermore, when the size of the materials goes down to the nanoscale, owing to the large surface tension and molar surface area compared to bulk materials, the solubility is greatly enhanced. The size effect on the solubility can be quantified by:[35] $\log K_{SP,NCs} = \log K_{SP,bulk} + 2\gamma A_m/[3\log(RT)]$, where K_{SP}, γ, and A_m are the solubility product, surface tension, and molar surface area ($m^2\ mol^{-1}$) of the solute, respectively. The size-enhanced difference in the solubility products should result in the acceleration of the cation exchange as observed from the NCs.[37] Nevertheless, it is counter-intuitive that such a complete cation-exchange reaction occurs under the condition that the concentration of potassium is much higher than that of sodium. Therefore, there must be another driving force to determine the thermodynamically favorable direction in the cation exchange reaction. Experimental results reveal that in the non-equilibrium solution reactions, $NaLnF_4$ preferentially crystallizes in the cubic phase as *α-NaLnF₄*, a high temperature metastable phase. However, beyond a certain size, owing to thermodynamic instability, this metastable phase inevitably transforms into the hexagonal one, which is a stable one at low temperature.[39] Therefore, hexagonal $NaLnF_4$ NCs that are more thermodynamically stable compared to cubic $KLnF_4$ may act as the seed nuclei to accelerate *in situ* cation exchange between potassium and sodium as well as the corresponding cubic to hexagonal phase transformation.

The possible process of *in situ* cation exchange between potassium and sodium and phase transformation from cubic to hexagonal is schematically illustrated in Fig. 4. In the first stage of the reaction [see Fig. 4(a)], the oleic phase consisting of OA, ethanol, sodium oleate, potassium oleate, and lanthanide oleate and the aqueous phase containing water, ethanol, and F^- are formed in the LSS reaction system. At a temperature above 180 °C, Ln^{3+} reacts with Na^+, K^+, and F^- to form hexagonal $NaLnF_4$ and cubic $KLnF_4$ particles simultaneously at the interfaces between the oleic and aqueous phases. The *in situ* generated oleic acid molecules adsorb on the surface of the particles and these oleophilic particles are monodispersed in the oleic phase. In this stage, both hexagonal $NaLnF_4$ and cubic $KLnF_4$ particles compete to grow until all the Ln^{3+} is completely depleted. If the hexagonal $NaLnF_4$ and cubic $KLnF_4$ particles are prepared separately, they will precipitate from the solution at the bottom of the autoclave. However, when both Na^+ and K^+ are added to the system, the reaction is quite different. When the

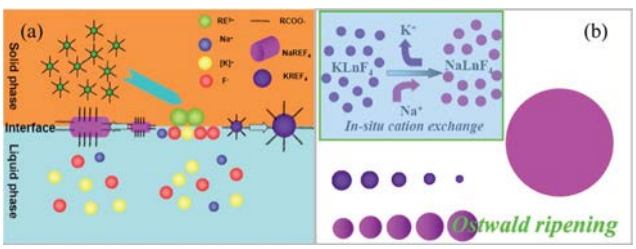

Fig. 4 A schematic illustration of *in situ* cation exchange between potassium and sodium and the phase transformation from cubic to hexagonal phase.

superfluous sodium is linked to the surface of cubic $KLnF_4$ particles, *in situ* cation exchange between potassium and sodium takes place immediately [see the inset of Fig. 4(b)]. Consequently, the cubic $KLnF_4$ particles become a metastable phase and are partly converted into cubic $NaLnF_4$. The cubic $NaLnF_4$ obtained *via* cation exchange cannot exist in a stable manner during long reactions. The existing stable hexagonal $NaLnF_4$ particles will act as seed nuclei to deplete them and grow continuously since the phase transformation from cubic to hexagonal $NaLnF_4$ can occur easily by Ostwald ripening [see Fig. 4(b)], resulting from the high solubility of metastable cubic $NaLnF_4$ with high free energy.[20]

The mechanism of the nucleation and size tuning of $NaLnF_4$ NCs described above can be verified by considering the dependence of the nucleation rate on the precursor concentration. In the solution controlled synthesis where the nucleation and ensuing growth are separated, Ostwald ripening is slow and the final NC size is determined by the number of seed nuclei. In this case, the final NC size is a good measure of the nucleation rate,[40–42]

$$\frac{dN}{dt} \propto r^{-3}, \tag{1}$$

where r is the mean radius of the NC. On the other hand, according to the classical nucleation theory, the nucleation rate is expressed as follows:

$$\frac{dN}{dt} = A\exp\left(-\frac{\Delta G^N}{RT}\right), \tag{2}$$

where, $\Delta G^N = 16\pi\gamma^3 V_m/3(RT\ln S)^2$ is the activation free energy, A is the preexponential factor, γ is the specific surface energy, and V_m is the molar volume. S is supersaturation, defined as the ratio between the monomer concentration and monomer concentration in equilibrium with the bulk solid phase (that is, solubility of the bulk solid) determined by the concentration of seed nuclei. Let $B = 16\pi\gamma^3 V_m^2/3(RT)^2$. We can rewrite the above eqn (1) as

$$\ln\frac{dN}{dt} = \ln A - B/(\ln S)^2 \propto 3\ln r. \tag{3}$$

This equation shows that the final size of the NCs depends strongly on the seed nuclei and decreases as the latter is increased.

Previously, Mai *et al.*[39] revealed that for light Ln^{3+} ions such as Gd^{3+}, Sm^{3+}, and Nd^{3+} with large ionic radii, the critical sizes beyond which cubic $NaLnF_4$ NCs were thermodynamically unstable to transform into the hexagonal phase were very small. Hence, hexagonal $NaGdF_4$, $NaSmF_4$ and $NaNdF_4$ were formed under mild conditions, even at room temperature and for a short time. Hence, it can be imagined that stable hexagonal particles form immediately in the initial stage of *in situ* cation exchange between potassium and sodium in the system containing Na, K, Gd, and F. As soon as the stable hexagonal $NaGdF_4$ particles form, they serve as seed nuclei to deplete cubic $NaGdF_4$ produced *via in situ* cation exchange of $KGdF_4$ by Na^+. In this process, the nucleation and growth of the final hexagonal $NaGdF_4$ are temporally separated and the number of $NaGdF_4$ seed nuclei is determined approximately by the Na^+ concentration (denoted as $[Na^+]$). If we vary the Na^+ concentration, $S \propto [Na^+]$ and eqn (3) can be expressed as

$$\ln\frac{dN}{dt} = \ln A - B/(\ln[Na^+])^2 \propto 3\ln r. \tag{4}$$

This equation predicts that the final size of the $NaGdF_4$ NCs decreases if the Na^+ concentration in the precursors increases. It is consistent with our experimental results (see Fig. 3 and its inset).

On the contrary, for heavy Ln^{3+}ions (Dy^{3+}–Lu^{3+}) and Y^{3+} which have rather big critical sizes, it usually requires at least 20 h at below 230 °C to complete the phase transformation of the thermodynamically unstable $NaLnF_4$ cubic phase to the pure hexagonal one.[39] No stable hexagonal particles form in the initial stage, and the nucleation and growth of the final hexagonal $NaYF_4$ and $NaYbF_4$ are not temporally separated in the Na–K–Yb–F and Na–K–Yb–F systems. Hence the number of $NaYF_4$ and $NaYbF_4$ seed nuclei cannot be considered to be proportional to the Na^+ concentrations. As a result, the corresponding size-tuning phenomena disappear. Recently, Liu *et al.* demonstrated that when doping Gd^{3+}, Sm^{3+}, or Nd^{3+} with a content of over 30%, it took only 2 h to obtain hexagonal Gd^{3+} doped $NaYF_4$ even at 200 °C.[3] The results imply that stable hexagonal particles may also form quickly in the initial stage of *in situ* cation exchange between potassium and sodium in the Na–K–Yb–F and Na–K–Yb–F systems *via* Gd^{3+} doping. The reoccurrence of the size-tuning phenomena in the two systems after Gd^{3+} doping

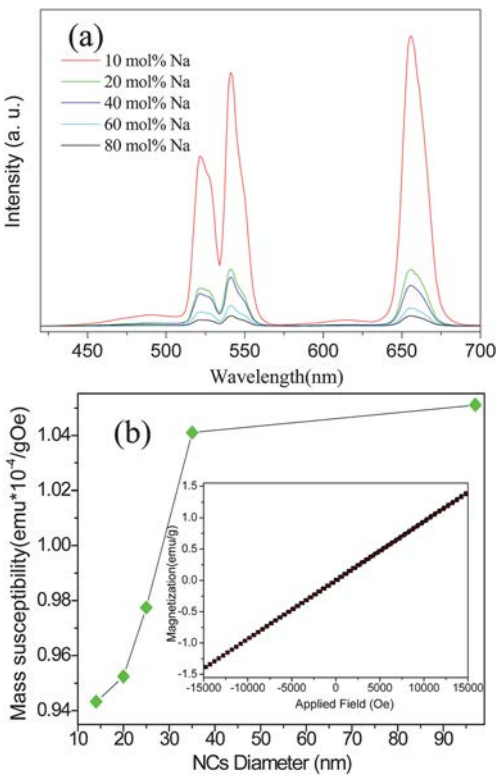

Fig. 5 (a) The UC emission intensity of Er^{3+} ions and (b) the magnetic mass susceptibility in the 0.5 mol% Er^{3+} doped $NaYb_{0.1}Gd_{0.9}F_4$ NCs samples with different sizes synthesized at 180 °C for 20 h using precursors with potassium : sodium molar ratios of 90 : 10, 80 : 20, 60 : 40, 40 : 60, and 20 : 80. The inset in (b) shows typical magnetization *vs.* magnetic field of $NaYb_{0.1}Gd_{0.9}F_4$ NCs measured at room temperature.

further reveals that stable hexagonal particles serving as seed nuclei that lead to the temporal separation of nucleation and growth of the final products play a key role in changing the size of the $NaLnF_4$ nanostructures during *in situ* cation exchange between potassium and sodium and the corresponding cubic to hexagonal phase transformation.

As aforementioned, Liu and co-workers demonstrated that the size and phases of $NaYF_4$ NCs could be tuned by introducing trivalent light Ln^{3+} dopant ions such as Gd^{3+}, Sm^{3+} and Nd^{3+}.[3] Considering the similarity between the experimental results of Liu *et al.* and ours, we consider that the nucleation controlled growth may also play a key role in changing the size and phase of $NaYF_4$ *via* Ln^{3+} doping. According to Liu's first-principle calculation which reveals that $NaYF_4$ is more energetically stable than $NaGdF_4$ in the cubic phase, we consider that there may be two ways to tune the phase and size of the products. One is that Y^{3+} and Gd^{3+} react with Na^+ and F^- separately to form hexagonal $NaGdF_4$ and cubic $NaYF_4$ particles simultaneously. The hexagonal $NaGdF_4$ particles serve as seed nuclei to accelerate the transformation of the cubic $NaYF_4$ to the hexagonal one. The other is that when Y^{3+} and Gd^{3+} react separately with Na^+ and F^- in the SSL reaction system in the initial stage, cubic $NaYF_4$ particles form preferentially. Because of the inter-miscibility of Ln^{3+} ions, fast cation exchange between Y^{3+} and Gd^3 occurs on the nanoscale, accompanied by the cubic $NaYF_4$ particles immediately doped with Gd^{3+} ions.[37] This change decreases the critical size for the transformation of the cubic to hexagonal phase and results in the accelerated formation of hexagonal $NaYF_4$ particles. As soon as the stable hexagonal $NaYF_4$ particles are formed, they act as seed nuclei to accelerate the transformation of the cubic $NaYF_4$ to the hexagonal one in the reaction. In both cases, one can find that the number of hexagonal $NaLnF_4$ particles as seed nuclei depends exclusively on the Gd^{3+} doping concentration.

3.3 Tunable UC emission and paramagnetism in hexagonal $NaLnF_4$ NCs

It should be stressed that the $NaLnF_4$ NCs with adjustable sizes between 100 and 10 nm produced by *in situ* cation exchange have almost uniform compositions. This is highly desirable in order to understand the size-dependent properties. Fig. 5(a) shows the UC emission intensity of Er^{3+} ions in Er^{3+} doped $NaYb_{0.1}Gd_{0.9}F_4$ NCs with different sizes synthesized at 180 °C for 20 h using precursors with potassium : sodium molar ratios of 90 : 10, 80 : 20, 60 : 40, and 40 : 60; 20 : 80. With reduced crystal sizes of the NCs and when the sodium contents in the precursors are from 20 to 80%, the UC emission intensity is notably depressed. The decreased emission intensity is primarily attributed to the increased surface quenching sites in smaller NCs, which can enhance nonradiative energy transfer of the luminescent Ln^{3+} ions.[3,43] The inset in Fig. 5(b) shows typical magnetization as

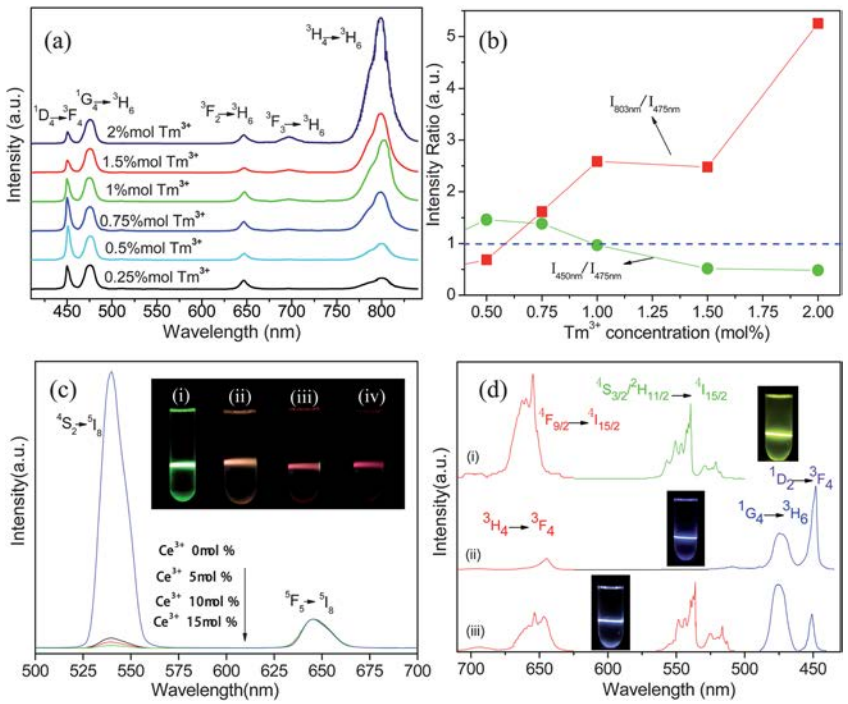

Fig. 6 (a) Room temperature normalized UC spectra of Yb^{3+}–Tm^{3+} co-doped $NaY_{0.55}Gd_{0.45}F_4$ NCs with different Tm^{3+} doping concentrations under the excitation of a 980 nm laser with an output power of about 1.0 W. All the spectra are normalized by the peak intensity at 475 nm. (b) The corresponding dependences of peak intensity ratio of 450/475 nm and 803/475 nm on Tm^{3+} doping concentrations in Yb^{3+}–Tm^{3+} co-doped $NaY_{0.55}Gd_{0.45}F_4$ NCs. (c) Normalized UC spectra of the 0.25 mol% Ho^{3+} doped $NaYb_{0.55}Gd_{0.45}F_4$ NCs co-doping with different Ce^{3+} concentrations under excitation by a 980 nm laser with an output power of about 1.0 W. All the spectra are normalized by the peak intensity at 650 nm. The inset is digital photographs of $NaYb_{0.55}Gd_{0.45}F_4$ NCs doped with (i) 0.25 mol% Ho^{3+} and 0 mol% Ce^{3+}, (ii) 0.25 mol% Ho^{3+} and 5 mol% Ce^{3+}, (iii) 0.25 mol% Ho^{3+} and 10 mol% Ce^{3+} and (iv) 0.25 mol% Ho^{3+} and 15 mol% Ce^{3+}. (d) Room temperature UC spectra and digital photographs of $NaY_{0.55}Gd_{0.45}F_4$ NCs doped with (i) 0.5 mol% Tm^{3+} and 20 mol% Yb^{3+}, (ii) 0.5 mol% Er^{3+} and 20 mol% Yb^{3+}, and (iii) 0.5 mol% Tm^{3+}, 0.125 mol% Er^{3+} and 20 mol% Yb^{3+}, respectively, under excitation by a 980 nm laser.

a function of applied magnetic field of Er^{3+} doped $NaYb_{0.1}Gd_{0.9}F_4$ NCs measured on a vibrating sample magnetometer with an applied field from −15 to 15 kOe. The NCs show obvious paramagnetism and it is unlike the behavior of Gd atoms which exhibit ferromagnetic behavior below 289 K. The paramagnetism in Er^{3+} doped $NaYb_{0.1}Gd_{0.9}F_4$ NCs can be ascribed to that the magnetic moments associated with Gd^{3+} are all localized and noninteracting.[18,44,45] Interestingly, as shown in Fig. 5(b), the magnetic mass susceptibility of the Er^{3+} doped $NaYb_{0.1}Gd_{0.9}F_4$ NCs is also size-dependent. Although the origin of size-dependent paramagnetic properties in these NCs is not clear, it likely originates from the unique surface effects of the NCs. In our experiments, Ln^{3+} ions such as Yb^{3+}, Tm^{3+}, Er^{3+}, Ho^{3+}, and Ce^{3+} below 15 mol% cannot yield size tuning effects in hexagonal $NaLnF_4$ NCs *via in situ* cation exchange. However, addition of these elements at a suitable concentration markedly induces color change in the UC emission under the excitation of a 980 nm laser. For example, by doping with Tm^{3+} with concentrations from 0.5 to 2 mol%, luminescent switching originating from the saturation effect[46] between different UC emission wavelengths at 800, 480, and 450 nm, which originate from the $^1D_2 \rightarrow {}^3F_4$, $^1G_4 \rightarrow {}^3H_6$ and $^3H_4 \rightarrow {}^3H_6$ transitions of Tm^{3+} ions, respectively, can be observed from Yb^{3+}–Tm^{3+} co-doped $NaY_{0.55}Gd_{0.45}F_4$ NCs [see Fig. 6(a) and (b)]. By doping with Ce^{3+} concentrations, the UC color output from green to red can be observed from Ho^{3+} doped $NaYb_{0.55}Gd_{0.45}F_4$ NCs [see Fig. 6(c)]. Moreover, the Er^{3+}–Yb^{3+}–Tm^{3+} tri-doped $NaY_{0.55}Gd_{0.45}F_4$ NCs lead to an adjustable balance of RGB intensities, allowing the tri-doped $NaY_{0.55}Gd_{0.45}F_4$ NCs to exhibit white UC emission [see Fig. 6d)]. Considering that Gd^{3+} is an ideal paramagnetic relaxation agent used in magnetic resonance imaging because of its large magnetic moment and nanosecond time scale electronic relaxation time, it is believed that the multifunctional $NaLnF_4$ NCs produced by *in situ* cation exchange giving tunable multi-color UC emission and paramagnetism have potential applications in color displays, bioseparation, and optical–magnetic dual modal nanoprobes in biomedical imaging.

4. Conclusions

Cation exchange between potassium and sodium on the nanoscale takes place irreversibly in the formation of $NaLnF_4$ particles when cubic $KLnF_4$ NCs are exposed to sodium ions due to the difference of the solubility constants and thermodynamic stability of the reactants and products. The stable hexagonal $NaLnF_4$ particles can act as seed nuclei to control the nucleation rate and size of final NCs during *in situ* cation exchange between potassium and sodium as well as the corresponding cubic to hexagonal phase transformation. The unusual cation exchange reaction provides not only valuable insights into the growth dynamics of Ln^{3+} doping-induced size tuning and phase transformation in $NaYF_4$ and alkaline-earth fluoride NCs, but also an approach to prepare high-quality multifunctional $NaLnF_4$ NCs with tunable paramagnetism and multi-color UC emission.

Acknowledgements

This work was supported by the Grants from National Natural Science Foundation of China (No.10802071), the Cultivation Fund of the Key Scientific and Technical Innovation Project (No.708068), Ministry of Education of China, Hong Kong Innovation and Technology Support Program (No. ITS/008/10), and City University of Hong Kong Strategic Research Grant No. 7008009.

References

1 F. Auzel, *Chem. Rev.*, 2004, **104**, 139–174.
2 J. Hao and J. Gao, *Appl. Phys. Lett.*, 2004, **85**, 3720.
3 F. Wang, Y. Han, C. Lim, Y. Lu, J. Wang, J. Xu, H. Chen, C. Zhang, M. Hong and X. Liu, *Nature*, 2010, **463**, 1061–1065.
4 B. van der Ende, L. Aartsa and A. Meijerink, *Phys. Chem. Chem. Phys.*, 2009, **11**, 11081–11095.
5 F. Wang and X. Liu, *Chem. Soc. Rev.*, 2009, **38**, 976–989.
6 C. Li and J. Lin, *J. Mater. Chem.*, 2010, **20**, 6831–6847.
7 L. D. Carlos, R. A. S. Ferreira, V. de Zea Bermudez, B. Julián-López and P. Escribano, *Chem. Soc. Rev.*, 2011, **40**, 536.
8 J. Stouwdam and F. van Veggel, *Nano Lett.*, 2002, **2**, 733–737.
9 S. Heer, K. Kmpe, H. Güdel and M. Haase, *Adv. Mater.*, 2004, **16**, 2102–2105.
10 J. Zeng, J. Su, Z. Li, R. Yan and Y. Li, *Adv. Mater.*, 2005, **17**, 2119–2123.
11 F. Zhang, Y. Wan, T. Yu, Y. Shi, S. Xie, Y. Li, L. Xu, B. Tu and D. Zhao, *Angew. Chem.*, 2007, **119**, 8122–8125.
12 J. Boyer, L. Cuccia and J. Capobianco, *Nano Lett.*, 2007, **7**, 847–852.
13 F. Wang and X. Liu, *J. Am. Chem. Soc.*, 2008, **130**, 5642–5643.
14 R. Kumar, M. Nyk, T. Ohulchanskyy, C. Flask and P. Prasad, *Adv. Funct. Mater.*, 2009, **19**, 853–859.
15 V. Mahalingam, F. Vetrone, R. Naccache, A. Speghini and J. Capobianco, *Adv. Mater.*, 2009, **21**, 4025.
16 Y. Park, J. Kim, K. Lee, K. Jeon, H. Na, J. Yu, H. Kim, N. Lee, S. Choi and S. Baik, *Adv. Mater.*, 2009, **21**, 4467–4471.
17 L. W. Yang, H. L. Han, Y. Y. Zhang and J. X. Zhong, *J. Phys. Chem. C*, 2009, **113**, 18995.
18 L. W. Yang, Y. Y. Zhang, J. J. Li, Y. Li, J. X. Zhong and P. K. Chu, *Nanoscale*, 2010, **2**, 2805–2810.
19 J. Hao, Y. Zhang and X. Wei, *Angew. Chem., Int. Ed.*, 2011, **50**, 6876.
20 L. W. Yang, Y. C. Li, S. X. Yu, J. H. Hao, J. X. Zhong and P. K. Chu, *Chem. Commun.*, 2011, **47**, 12544–12546.
21 D. Chen, Y. Yu, F. Huang, P. Huang, A. Yang and Y. Wang, *J. Am. Chem. Soc.*, 2010, **132**, 9976.
22 J. Zhou, Y. Sun, X. Du, L. Xiong, H. Hu and F. Li, *Biomaterials*, 2010, **31**, 3287–3295.
23 X. Wang, X. Yan and C. Kan, *J. Mater. Chem.*, 2011, **21**, 4251–4256.
24 Q. Liu, Y. Sun, C. Li, J. Zhou, T. Yang, X. Zhang, T. Yi, D. Wu and F. Li, *ACS Nano*, 2011, **5**, 3146–3157.
25 Y. Sun, M. Yu, S. Liang, Y. Zhang, C. Li, T. Mou, W. Yang, X. Zhang, B. Li and C. Huang, *Biomaterials*, 2011, **32**, 2999–3007.
26 J. Zhou, M. Yu, Y. Sun, X. Zhang, X. Zhu, Z. Wu, D. Wu and F. Li, *Biomaterials*, 2011, **32**, 1148.
27 Y. Liu, D. Tu, H. Zhu, R. Li, W. Luo and X. Chen, *Adv. Mater.*, 2010, **22**, 3266–3271.
28 Z. L. Wang, J. H. Hao and H. L. W. Chan, *J. Mater. Chem.*, 2010, **20**, 3178–3185.
29 D. Chen, Y. Yu, F. Huang, A. Yang and Y. Wang, *J. Mater. Chem.*, 2011, **21**, 6186.
30 D. Chen, Y. Yu, F. Huang and Y. Wang, *Chem. Commun.*, 2011, **47**, 2601–2603.
31 D. H. Son, S. M. Hughes, Y. Yin and A. Paul Alivisatos, *Science*, 2004, **306**, 1009.
32 R. D. Robinson, B. Sadtler, D. O. Demchenko, C. K. Erdonmez, L. W. Wang and A. P. Alivisatos, *Science*, 2007, **317**, 355.
33 U. Jeong, J. U. Kim, Y. Xia and Z. Y. Li, *Nano Lett.*, 2005, **5**, 937–942.
34 J. M. Pietryga, D. J. Werder, D. J. Williams, J. L. Casson, R. D. Schaller, V. I. Klimov and J. A. Hollingsworth, *J. Am. Chem. Soc.*, 2008, **130**, 4879–4885.
35 S. E. Wark, C. H. Hsia and D. H. Son, *J. Am. Chem. Soc.*, 2008, **130**, 9550–9555.
36 G. D. Moon, S. Ko, Y. Xia and U. Jeong, *ACS Nano*, 2010, **4**, 2307–2319.

37 C. Dong and F. C. J. M. van Veggel, *ACS Nano*, 2009, **3**, 123–130.
38 S. Zeng, G. Ren, C. Xu and Q. Yang, *CrystEngComm*, 2011, **13**, 1384–1390.
39 H. X. Mai, Y. W. Zhang, R. Si, Z. G. Yan, L. Sun, L. P. You and C. H. Yan, *J. Am. Chem. Soc.*, 2006, **128**, 6426–6436.
40 M. A. Hines and G. D. Scholes, *Adv. Mater.*, 2003, **15**, 1844–1849.
41 M. V. Kovalenko, W. Heiss, E. V. Shevchenko, J. S. Lee, H. Schwinghammer, A. P. Alivisatos and D. V. Talapin, *J. Am. Chem. Soc.*, 2007, **129**, 11354–11355.
42 E. V. Shevchenko, D. V. Talapin, H. Schnablegger, A. Kornowski, Festin, P. Svedlindh, M. Haase and H. Weller, *J. Am. Chem. Soc.*, 2003, **125**, 9090–9101.
43 F. Wang, J. Wang and X. Liu, *Angew. Chem., Int. Ed.*, 2010, **49**, 7456–7460.
44 H. Wong, H. Chan and J. Hao, *Opt. Express*, 2009, **18**, 6123–6130.
45 H. Wong, H. Chan and J. Hao, *Appl. Phys. Lett.*, 2009, **95**, 022512.
46 C. Jacinto, M. Vermelho, E. Gouveia, M. de Araujo, P. Udo, N. Astrath and M. Baesso, *Appl. Phys. Lett.*, 2007, **91**, 071102–071102.

